minerals

MDPI

Article

A Novel Comprehensive Detection Method for the Dynamic Characteristics of Coalface Overburden: A Case Study in China

Wei Zhang [1,2,3,4], Zhi Yang [5], Dongsheng Zhang [6,*], Xufeng Wang [5], Peng Li [5] and Mengtang Xu [7]

1 IoT Perception Mine Research Center, National and Local Joint Engineering Laboratory of Internet Application Technology on Mine, China University of Mining & Technology, Xuzhou 221008, China; zhangwei@cumt.edu.cn
2 State and Local Joint Engineering Laboratory for Gas Drainage & Ground Control of Deep Mines, Henan Polytechnic University, Jiaozuo 454000, China
3 Key Laboratory of Safety and High-Efficiency Coal Mining, Ministry of Education, Anhui University of Science & Technology, Huainan 232001, China
4 State Key Laboratory of Coal Mine Disaster Dynamics and Control, Chongqing University, Chongqing 400044, China
5 School of Mines, China University of Mining & Technology, Xuzhou 221116, China; yangzhi@cumt.edu.cn (Z.Y.); wangxufeng@cumt.edu.cn (X.W.); cumt_lp@cumt.edu.cn (P.L.)
6 State Key Laboratory of Coal Resources and Safe Mining, China University of Mining & Technology, Xuzhou 221116, China
7 Institute of Mining Engineering, Guizhou Institute of Technology, Guiyang 550003, China; xmtcumt@126.com
* Correspondence: dshzhang123@cumt.edu.cn; Tel./Fax: +86-516-8359-1725

Academic Editor: Abbas Taheri
Received: 24 November 2016; Accepted: 29 January 2017; Published: 15 February 2017

Abstract: Accurate and efficient acquisition of information about the dynamic characteristics of coalface overburden can provide an important theoretical basis for green mining in coal producing regions in western China. In this study, a novel method for comprehensively detecting the dynamic behavior of coalface overburden is proposed in order to address deficiencies of the existing detection methods. The new method combines surface radon measurement, overburden borehole imaging, and underground pressure observation into a comprehensive detection technology system, resulting in spatial and temporal integration of surface, overburden, and underground detection. To examine the feasibility of the proposed method, a field experiment was carried out at #1103 coalface in the Suancigou Coal Mine, which is operated by the Inner Mongolia Yitai Coal Co. Ltd. The results of the three approaches are largely consistent and they complement one another. But it must be pointed out that this method needs to be further improved by more field experiments. Based on the experimental results, a technique for forced caving by presplit blasting of the overburden was developed and then implemented to #1103 coalface. The practical use of the technique led to good results: it effectively prevented roof-associated accidents by controlling the first weighting step to about 82 m, contributing to safe and efficient mining; coal production was expected to increase about 126 kilotons.

Keywords: coalface overburden; dynamic characteristics; comprehensive detection method; spatial and temporal integration; forced caving by presplit blasting

1. Introduction

Coal resources in eastern China are depleting, and the mining areas of central China are subjected to resource and environmental constraints [1]. In response, a general strategy was laid out in China's

12th Five-Year Plan (2011–2015) for the Development of the Coal Industry, which stated that "coal resource development will be controlled in the eastern part, moderated in the central part, and accelerated in the western part of the country" [2]. Under this strategy, the focus of national coal resource development has rapidly shifted to the ecologically fragile arid and semi-arid regions in western China [3,4]. In these regions large coal resource basins have recently emerged, including the Shanbei, Huanglong, Shendong, Ningdong, and Xinjiang bases. Coal seams in the western mining areas are typically thick, shallow, and overlain with thin bedrock and thick soil. The period from 2002 to 2012 was named "The Golden Decade of China's Coal Industry" [5]. During this period, intense and extensive longwall mining method was practiced on a large scale. Consequently, breakage of overburden directly affected the surface of a coalface and there was an increased likelihood that the overburden would subside entirely, which induced strong mine ground pressure and significant deformation of the surface of the coalface [6]. Further, underground mining can easily cause damage to aquifers, loss of shallow groundwater, and vegetation degradation, making fragile ecologies more vulnerable to catastrophic damage. Environmental harm caused by coal mining is currently attracting widespread attention from multiple sectors of society. As laid out in the Outline of the 13th Five-Year Plan (2016–2020) for the National Economic and Social Development of the People's Republic of China, "...efforts are needed to promote clean coal technology and efficient use of coal. The coal resource development will be restricted in the eastern part of the country and be controlled in the central and northeastern regions, while that in the western regions will be given priority. Green mining techniques and technological transformation will be promoted in large coal resource basins..." [7]. It is also important to consider the context of structural reform of the supply side of the national coal market. In this regard, accurate and efficient acquisition of information about the dynamic characteristics of coalface overburden (DCCO) can provide a theoretical basis for scientific mining in coal producing regions in western China. This is in accordance with the definition of scientific mining given by Qian [8], an academician of the Chinese Academy of Engineering: scientific mining refers to mining using technology that can be implemented to achieve efficient coal extraction without causing safety accidents, doing harm to the environment, or wasting resources.

Existing engineering practice research on the dynamic behavior of coalface overburden does not include a detection method that is practicable, efficient, and easy to implement. The most commonly used methods include remote sensing satellite-based monitoring [9–11], overburden borehole imaging (OBI) [12–14], geophysical and geochemical exploration [15–24], deep base point displacement metering [25,26], and underground pressure observation (UPO) [27–29]. If these methods are improperly used alone or in combination, the detection process may not produce satisfactory results because of mining geological conditions [30]. For example, mining-induced abutment pressure ahead of a coalface makes it impossible to monitor and accurately identify the overburden's state of motion throughout the mining process, which poses a major obstacle for effective implementation of safe and green mining technologies. Therefore, there is an urgent need to explore a comprehensive detection method (CDM) that can be used to capture valid, real-time information about the DCCO.

Radon (Rn) is a typical atmophile element with an atomic number of 86. Under normal conditions it occurs as radon gas, which is radioactive and noble. It is a decay product of $_{88}$Ra, which in turn is a decay product of $_{92}$U ($_{92}$U to $_{88}$Ra to $_{86}$Rn), i.e., $_{86}$Rn is the granddaughter of $_{92}$U. Radon is ubiquitous in the natural world, and is present in the atmosphere, soil, underground strata and coal seams, and groundwater [31]. It can move through or accumulate in micro cracks or pores. The concentration of radon is directly measurable by emanometers. These characteristics provide a scientific basis for surface radon measurement (SRM) above a coalface.

This study presents a novel CDM for the DCCO, with an aim of overcoming the limitations of existing methods. This novel method combines SRM, OBI, and UPO into a comprehensive detection technology system, enabling spatial and temporal integration of surface, overburden, and underground detection. To examine the feasibility of the method, it was applied to #1103 coalface in the Suancigou Coal Mine (SCM) of the Inner Mongolia Yitai Coal Co. Ltd (IMYCCL). A technique for forced caving by

presplit blasting (FCPB) was developed from this method, and then the technique was implemented at #1103 coalface. This technique allowed for safe and efficient mining at the coalface.

2. A Novel Comprehensive Detection Method

The novel CDM is easy to implement, highly efficient, very practical, and widely applicable [32]. Though the three methods which were applied were all known techniques, the CDM is an integrated innovation method. In other words, the three known techniques may complement one another, and eventually could overcome the uncertainty of traditional single detection method, which is the novel point of the CDM. The specific operations involved in on-site detection using this method are described below, and a schematic of the detection site is shown in Figure 1.

(a) Delineation of a surface detection area, based on the mining geological conditions of the underground coalface, which corresponds to the scope of the overburden to be detected.

(b) Layout of radon measurement lines (RMLs) at regular intervals within the delineated detection area. These lines should be perpendicular to the direction of movement of the coalface. Then, set radon measurement points (RMPs) at fixed intervals along the RMLs.

(c) Embedding of an inverted radon collector of the cumulative emanometer (CD-1/KZ-D02, KZNTD Company, Chengdu, China), at each RMP, 30 cm deep into the soil. After at least 4 h have passed, the radon collectors are taken out and quickly placed into the cumulative emanometer, pulse counting is performed, and the results are stored. The purpose of SRM is to forecast the position of breakage of the main roof in front of the coalface and to investigate the development of cracks in the ground surface.

(d) Drilling of a long borehole at a predetermined angle on the horizontal plane, into the roof above the solid coal. The mouth of the borehole should be located at the midpoint of the corresponding upper edge of the tailgate section that is covered by the vertical projection of the surface detection area. Then a set of borehole imaging instruments (TYGD10, HDMSD Company, Xuzhou, China) is used to continuously visualize the entire borehole wall. OBI is conducted to achieve real-time monitoring of the movement of the strata and the evolution of fractures in the overburden of the coalface.

(e) Installation of mine digital pressure gauges (YHY60, Uroica Company, Tai'an, China) on the hydraulic supports (HSs) to keep continuous records of the working resistances on the supports and store the values. Then a mine pressure data collector (FCH2G/1, Uroica Company, Tai'an, China) is used to gather the stored values via wireless infrared transmission. This procedure is intended for real-time analysis of the results of roof control as well as for the deformation, fracture, and movement of the overburden.

(f) Upload of the data from steps (c), (d), and (e) to a computer workstation using a USB cable, after all fieldwork is complete. After that, the DCCO can be derived from the results produced by the three approaches.

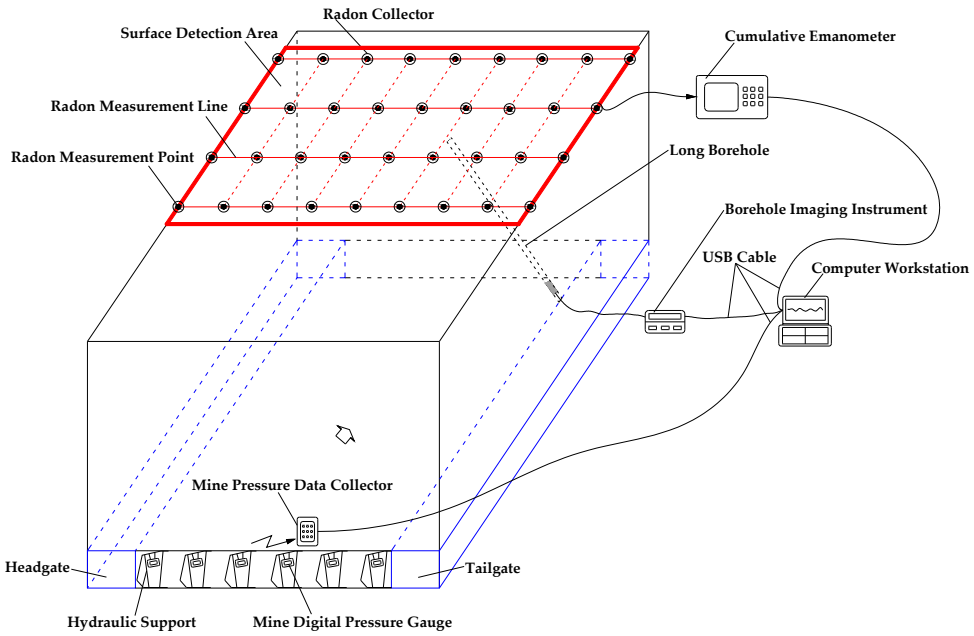

Figure 1. Schematic of the detection site.

3. Mine Overview and Mining Conditions

3.1. Mine Overview

Lying in the northeast part of Ordos City in Inner Mongolia, the SCM covers the central portion of the Jungar Coalfield, or the northwest corner of the southern detailed exploration area. SCM is located at 39°40′45″ N 111°09′06″ E/39°47′52″ N 111°14′38″ E. It covers an area of 76.5 km^2, and has an irregular boundary with a north–south extent of 11.5 km and an east-west extent of 5.7 km. The surface of the SCM is covered with loess and aeolian sand and is criss-crossed by gullies. This area ranges from +1230 to +1180 m in elevation, with a relative elevation difference of 50 m. Overall, its central and northern parts are higher than its eastern and western parts.

The SCM is a modern mega mine developed by IMYCCL. It has a design production capacity of 12 million tons per year and an estimated lifetime over 80 years. Development openings in the mine include vertical and sloping shafts, i.e., the main and auxiliary shafts are inclined while the ventilation shaft is vertical. The elevation of the mining level is +900 m. Three east-west directional main roadways were built to develop the whole mine. The panel is adopted to downwards exploit #6$_{up}$ and #6 coal seams, which means that the former is mined in advance of the latter.

3.2. Mining Conditions

The first mining zone of the SCM is #1 panel in its southern part, of which the first coalface is #1103 coalface. Figure 2 shows the stratigraphic column of first mining zone. #1103 coalface is 1500 m long along its strike and 300 m wide along its dip, and spans 450,000 m^2. The surface of the coalface ranges from +1126.8 to +1232.5 m in elevation. The floor below the coal seam ranges from +903.601 to +942.291 m in elevation. #6$_{up}$ coal seam ranges from 2.98 to 7.3 m thick, with an average of 5.08 m. Its dip angle averages 3° and ranges between 0° and 6°. The surrounding geological conditions are complex. The roof above the coal seam is comprised primarily of mudstone and coarse-grained sandstone and the floor below the coal seam is dominated by mudstone and siltstone. The retreating longwall mining method is used at this coalface to cut the entire height (5.0 m) of the coal seam along its strike. The roof is allowed to collapse entirely into the goaf.

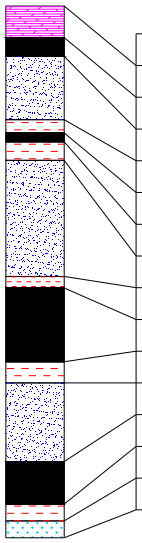

Succession	Lithology	Thickness	Remarks
1	Lime mudstone	5.43 m	/
2	Coal	3.26 m	#4 coal seam
3	Gritstone	10.5 m	/
4	Mudstone	2.30 m	/
5	Coal	1.44 m	#5 coal seam
6	Mudstone	3.21 m	/
7	Gritstone	33.0 m	Main roof
8	Mudstone	2.00 m	Immediate roof
9	Coal	12.7 m	#6_{up} coal seam
10	Mudstone	3.65 m	Immediate floor
11	Gritstone	13.6 m	Main floor
12	Coal	7.34 m	#6 coal seam
13	Mudstone	2.90 m	/
14	Medium-grained sandstone	4.15 m	/

Figure 2. Stratigraphic column of first mining zone.

4. Field Experiment and Analysis of the Results

4.1. Surface Radon Measurement

4.1.1. Radon Measurement Point Layout

The mining conditions of #1103 coalface were used to determine the layout of the RMPs: First, RMLs #1 through #4 were laid out parallel to, and in front of, the open-off cut at 20 m intervals, with the #1 RML being 40 m from the open-off cut. Then, RMPs #1 through #11 were laid out at 30 m intervals along each RML. Next, error evaluation points #1 through #3 were set at 75 m intervals along the centerline of the surface region above the coalface. Figure 3 depicts the layout of RMPs on the surface of #1103 coalface.

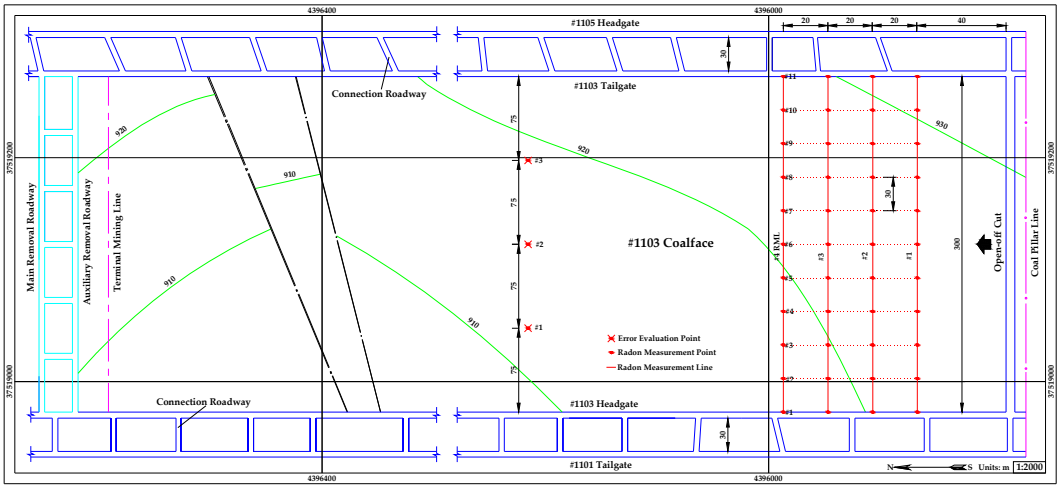

Figure 3. Layout of radon measurement points (RMPs) on the surface of #1103 coalface.

4.1.2. On-Site Measurement

After the RMPs were laid out, radon measurement was conducted on the surface of #1103 coalface. The following procedures were used: first, a pit that was 30 cm deep and 20 cm wide was dug at each RMP and an inverted radon collector was placed in each pit. After that, the pits were filled in with soil

and then covered with plastic films (Figure 4). Next, before mining began, in order to examine the statistical fluctuations in radioactivity, a one-week continuous radon measurement was performed at each of the three error evaluation points. As the coalface moved forward from the open-off cut, radon concentrations were measured once a day at the 44 RMPs along the four RMLs. Figure 5 shows the on-site measurement procedures. Under normal circumstances, the radon collectors can be taken out from the pits for measurement four hours after placement [33]. During this on-site measurement, each radon collector was embedded in the pit for 24 h and taken out for measurement once per day [34], due to limitations in the field conditions. The coalface kept advancing during the intervals.

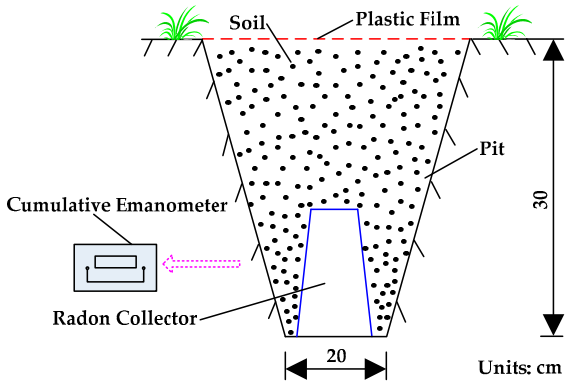

Figure 4. Schematic of a radon collector embedded in the pit at an RMP.

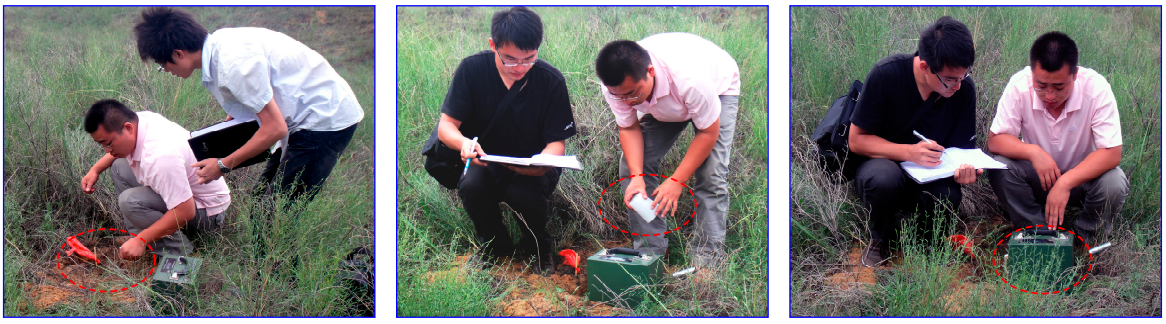

(**a**) (**b**) (**c**)

Figure 5. On-site measurement procedures: (**a**) digging a pit; (**b**) embedding a radon collector; (**c**) pulse counting.

4.2. Overburden Borehole Imaging

4.2.1. Borehole Layout Parameters

A borehole imaging station within #21 connection roadway, was set up approximately 100 m ahead of the open-off cut to predict the mode, position, and time of fracture of the overburden in front of the coalface. Its location was determined according to the actual mining conditions and in relation to the location of #1103 tailgate relative to #1105 headgate. The borehole was drilled at an angle of 33° on the horizontal plane, and its mouth was located at the midpoint of #21 connection roadway. The borehole's diameter was 40 mm and its length was 60.8 m. The vertical distance between its two ends was 33.1 m, as shown in Figure 6.

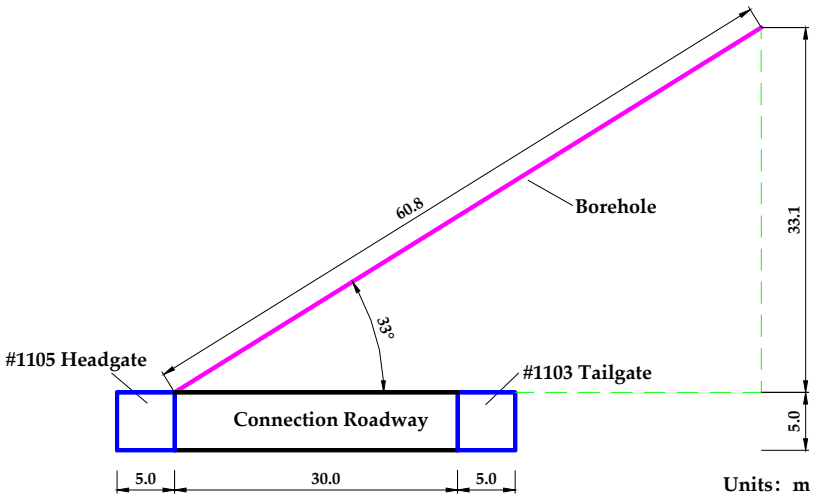

Figure 6. Schematic of borehole layout parameters.

4.2.2. Field Imaging

During the production, the borehole wall was imaged every time the coalface moved 10 m forward until the coalface was 100 m from the open-off cut. The borehole imaging instrument used in the field imaging consisted of four parts: the main equipment, auxiliary equipment, high-definition probe and supporting rods [35], as shown in Figure 7. The images of the borehole wall that the auxiliary equipment generated could be transmitted via the electric cable to the main equipment, appear on its display in real time, and are stored in the high-capacity memory card. A computer-based comparative analysis of the images can provide insights into the dynamic behavior of the overlying strata above the coal seam.

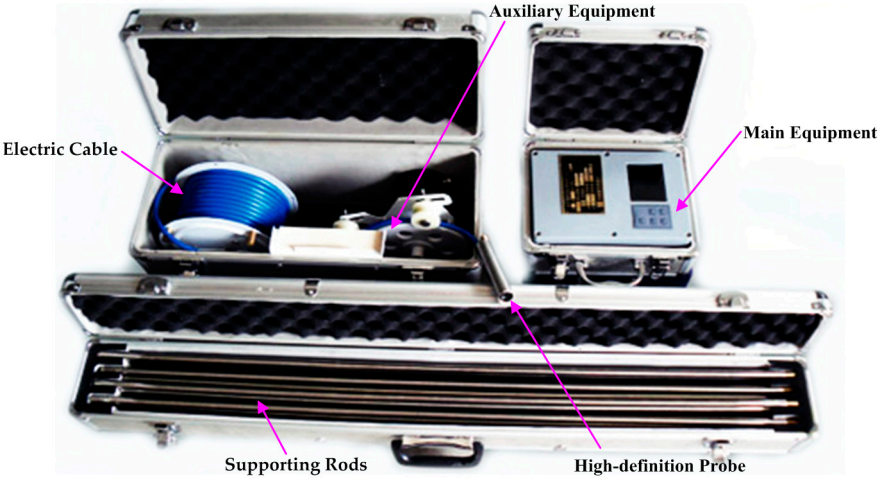

Figure 7. Structural composition of the borehole imaging instrument.

4.3. Underground Pressure Observation

4.3.1. Layout of Underground Observation Points

The coalface was divided, along its dip direction [36], into three observation areas to observe the underground pressure behavior in these areas. This can provide a basis for implementation of specific roof control measures. As shown in Figure 8, a total of 14 observation points were laid out in these areas: four observation points in the upper observation area (HSs #4, #17, #30, and #43), six

observation points in the middle observation area (HSs #56, #69, #82, #95, #108, and #121), and four observation points in the lower observation area (HSs #134, #147, #160, and #173).

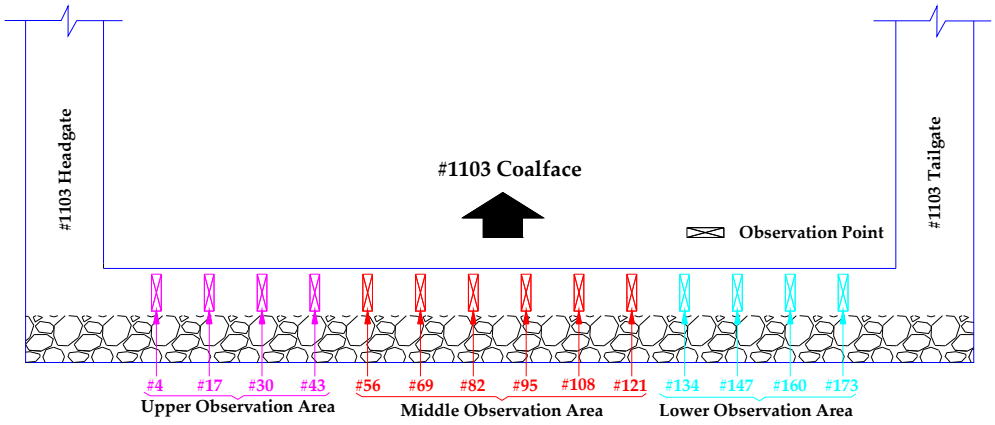

Figure 8. Layout of underground observation points.

4.3.2. Field Observation

A pressure recording system (KBJ-60III-1, Uroica Company, Tai'an, China) was used to continuously record the working resistance on the HSs. This system includes four major components: a mine digital pressure gauge, a mine pressure data collector, a wireless communication adapter, and a computer workstation (Figure 9). With two pressure taps, one mine digital pressure gauge can continuously measure the working resistance on the front and rear legs of a HS and simultaneously store the data. A coalface can be installed with between 1 and 24 mine digital pressure gauges and the pressure data generated by the different gauges can be gathered using one mine pressure data collector. The HSs (2400/5000-2×4412-1750, DBT Company, Lunen, Germany) installed in #1103 coalface are two-leg shield supports. In this field observation, the working resistances on both legs of each HS in #1103 coalface were recorded at 5 min intervals as the coalface advanced from the open-off cut. Meanwhile, there was monitoring of the roof and wall falling in the three observation areas to acquire real-time information about the underground pressure behavior in different locations of the coalface.

Figure 9. Schematic of the pressure recording system.

4.4. Analysis of Experimental Results

4.4.1. Results of Surface Radon Measurement

(1) Experimental error analysis

Radioactive materials are comprised of large radioactive atoms, whose radioactive decay is contingent and random. Therefore, a radioactive decay process frequently statistically fluctuates during actual measurement, which can cause a statistical fluctuation error and is the main source of experimental error [37,38]. In order to evaluate the degree of influence that the natural fluctuation error had on the measurements, three error evaluation points were laid out along the centerline of the surface

region above #1103 coalface. The radon concentration at the error evaluation point could be used as a sample, and the calculated results of the sample parameters are listed in Table 1, which include the average value, standard deviation and coefficient of variation. In examining Table 1, one can draw the conclusion that the degree of statistical fluctuation is relatively small in this field experiment, and the coefficients of variation of the sample parameters were mostly below 1%. Therefore, the experimental error will not significantly affect the subsequent measured data analysis.

Table 1. The calculated results of the sample parameters.

Error Evaluation Point	Average Value	Standard Deviation	Coefficient of Variation
#1	3675	32.34	0.88%
#2	3598	28.42	0.79%
#3	3680	33.12	0.90%

(2) Measured data analysis

The Daubechies wavelet was applied to further eliminate causes of error in the measured data. This wavelet uses a two-order discrete orthogonal wavelet transformation to handle the measured data. The measured data from the RMPs along RMLs #1 to #4 were plotted on a three-dimensional graph using MATLAB software and then the data set was smoothed through interpolation based on the grid density. Then the measured data was analyzed and interpreted, together with the actual progress of mining at #1103 coalface. Before mining began, the average background counts of radon at the upper and lower ends of the surface detection area were around 3720 and 3700, respectively, and radon background counts in the central part of the area was 3,660. Because the adjacent coalfaces #1101 and #1105 had already been arranged, lateral abutment pressure was larger at the two ends of #1103 coalface, which provided many mining-induced fracture channels for radon migration near the two ends. This caused the two ends to have values that measured higher than the values from the middle part. As the #1103 coalface progressed, the overburden began to move and deform and mining-induced tiny cracks that were parallel to the open-off cut arose in the corresponding surface area. When the coalface moved approximately 78 m forward (close to #3 RML), large through cracks developed in the surface along the dip direction of the coalface, as shown in Figure 10. At the same time, the counts measured at the RMPs along #3 RML peaked, as illustrated in Figure 11. The maximum counts near the upper and lower ends of the coalface were 4530 and 4511, respectively, an increase of 17.88% and 17.98% from the corresponding background values. The maximum count measured near the center was approximately 4320, a 15.28% increase from the background value. It is reasonable to infer from the results that the first breakage of the key strata in the main roof (which controlled the overburden's behavior) and the ensuing first weighting would soon occur at this coalface and the first weighting step would be larger than 78 m.

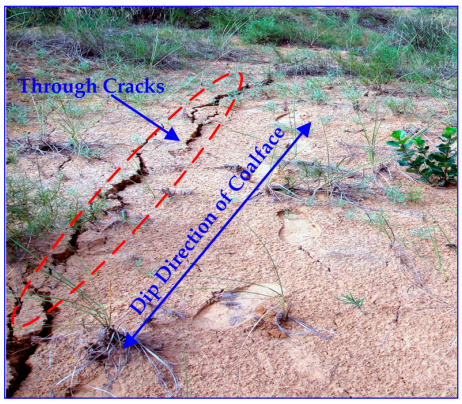

Figure 10. Through cracks in the surface.

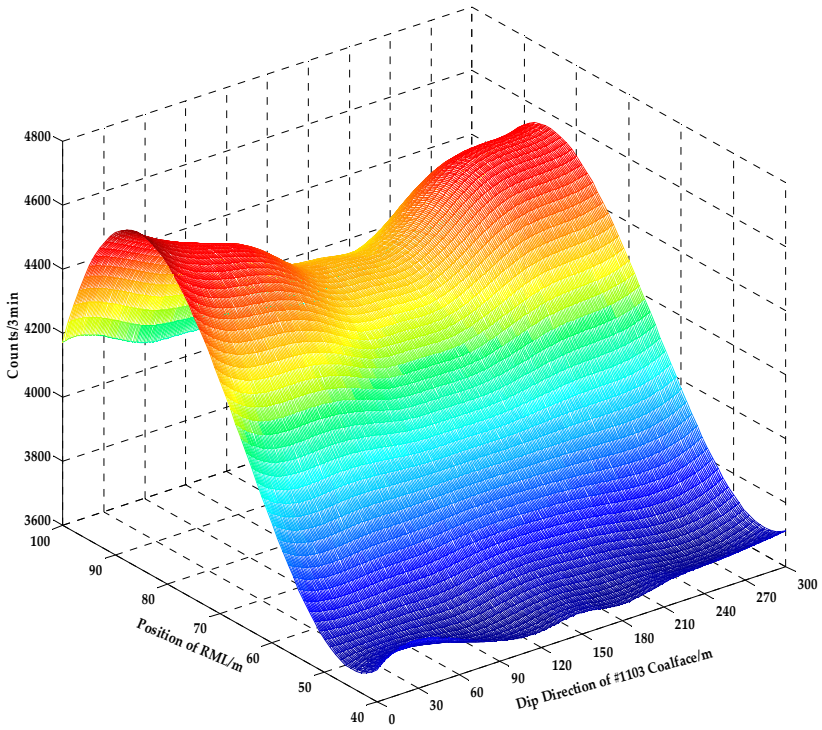

Figure 11. Radon counts from the RMPs.

4.4.2. Results of Overburden Borehole Imaging

Borehole imaging started when the #1103 coalface was 100 m behind the borehole, in order to avoid the influence of abutment pressure in front of the coalface. The development of mining-induced fractures in the borehole wall was monitored, and the resulting images were stored. Four characteristic points that can reveal characteristics of the overburden movement and deformation were selected on the borehole wall. They were located at the coal-rock interface (#1 characteristic point), 23 m from the borehole mouth (#2 characteristic point), 50 m from the borehole mouth (#3 characteristic point), and at the bottom of the borehole (#4 characteristic point). Figures 12–15 compare the images of the borehole wall that were taken at these points when the distances between the borehole mouth and the coalface were 100, 30, and 20 m. A 1.6 m thick layer of coal was left above the connection roadway where the borehole was located (5.0 m) because the height of this roadway is smaller than the point thickness (6.6 m) of the coal seam. Therefore, the borehole penetrated the coal-rock interface. During the imaging, the overburden around #1 characteristic point did not have a noticeable deformation, as depicted in Figure 12. At #2 characteristic point (Figure 13), the borehole wall did not exhibit significant deformations when the borehole mouth was still distant from the coalface. Only one tiny mining-induced fracture occurred when the borehole mouth was 30 m from the coalface. As the coalface progressed to a position 20 m from the borehole mouth, more and larger mining-induced fractures arose. Mining-induced fractures at #3 characteristic point (Figure 14) developed almost at the same time as those at #2 characteristic point, when the borehole mouth was 30 and 20 m from the coalface. Figure 15 shows that, as mining progressed, no significant deformation or fracture took place at the borehole bottom and the borehole wall did not undergo extensive fracture or dislocation. These results demonstrate that the overburden did not undergo significant deformation, fracture, or movement as the coalface advanced from the open-off cut to the position that was 20 m from the borehole mouth. Therefore, the first weighting step was predicted to exceed 80 m.

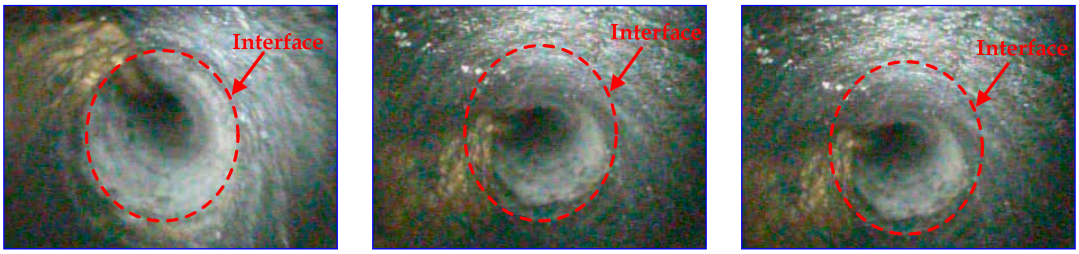

(**a**) (**b**) (**c**)

Figure 12. Images of the overburden around #1 characteristic point: (**a**) 100 m from the coalface; (**b**) 30 m from the coalface; (**c**) 20 m from the coalface.

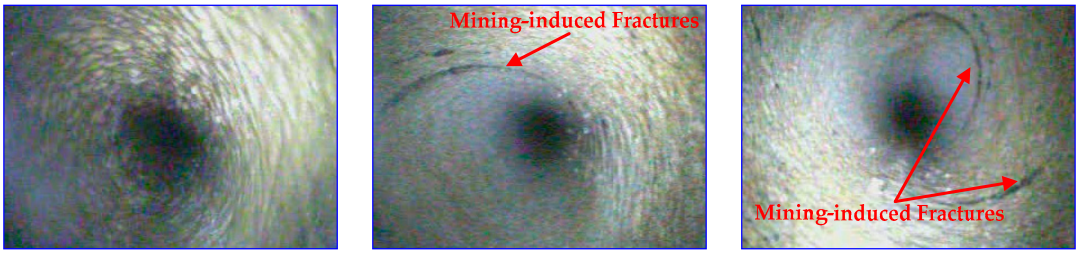

(**a**) (**b**) (**c**)

Figure 13. Images of the overburden around #2 characteristic point: (**a**) 100 m from the coalface; (**b**) 30 m from the coalface; (**c**) 20 m from the coalface.

(**a**) (**b**) (**c**)

Figure 14. Images of the overburden around #3 characteristic point: (**a**) 100 m from the coalface; (**b**) 30 m from the coalface; (**c**) 20 m from the coalface.

(**a**) (**b**) (**c**)

Figure 15. Images of the overburden at #4 characteristic point: (**a**) 100 m from the coalface; (**b**) 30 m from the coalface; (**c**) 20 m from the coalface.

4.4.3. Results of Underground Pressure Observation

Over three periods, the underground pressure was observed at #1103 coalface. In the first period, the coalface advanced from the open-off cut to the location 165 m ahead of it. In the second period, the coalface traveled from 217 m ahead of the open-off cut to 470 m ahead of the open-off cut. The third period started when the coalface was 1156 m ahead of the open-off cut and ended as it reached the terminal mining line. This study only analyzed the data observed before the first weighting occurred. Since #1103 coalface is the first coalface of #1 panel in the SCM, the mining progress was discontinuous and slow because of workers´ inexperience with operating the equipment and the need to run-in equipment. When the coalface was 60 m ahead of the open-off cut, the immediate roof above the goaf behind the coalface easily caved as the mining progressed, while the overlying main roof remained hanging above the goaf. The HSs in the upper observation area, middle observation area, and lower observation area were subject to stable working resistances, as illustrated in Figure 16. As mining progressed, rib fall, accompanied by cracking sounds, began to occur locally in the middle part of the coalface. Water constantly dropped from the roof above the HSs and advanced cave-ins of the immediate roof above the rib occurred. When the distance between the coalface and the open-off cut reached 75 m, the area of the hanging main roof expanded and the safety valves of many HSs opened. Working resistances acting upon the HSs in the three observation areas increased sharply (Figure 17), resulting in significant underground pressure behavior. The maximum working resistance was observed at 8790 kN (54.64 MPa), which is equivalent to 99.61% of the rated working resistance. The average dynamic load factor was calculated at 1.53. The first breakage of the main roof and ensuing first weighting were about to occur when the coalface moved 75 m forward, and the first weighting step exceeded 75 m.

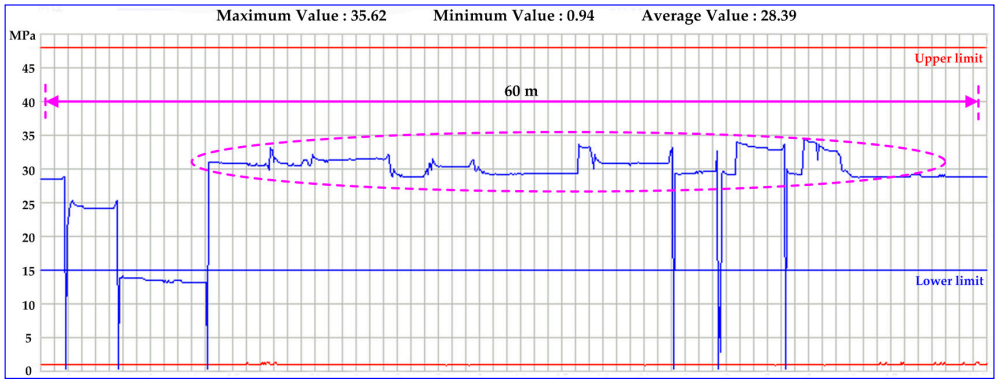

Figure 16. Working resistances on the hydraulic supports (HSs) when the coalface moved 60 m forward.

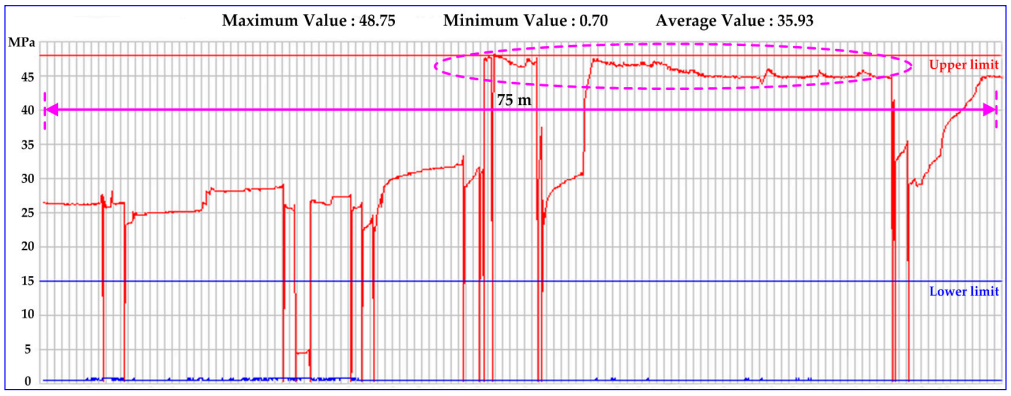

Figure 17. Working resistances on the HSs when the coalface moved 75 m forward.

5. A Technique for Forced Caving by Presplit Blasting

As the main roof above #1103 coalface was comprised of coarse-grained sandstone (33 m thick) that was too stable to cave easily, long segments of the main roof could be easily left hanging above the goaf. The experimental results from the on-site detection indicate that the first weighting step was relatively long. This, together with the experimental results, indicates that the first weighting could possibly cause extremely violent underground pressure behavior, which in turn could cause roof-associated accidents such as crushing of HSs and roof fall accidents. Therefore, a technique for FCPB of the overburden was developed and applied to #1103 coalface before the first weighting. By implementing the technique, roof-associated disasters were effectively prevented and the goal of safe production was achieved at this coalface.

5.1. Design Principles for the Technical Proposal

A proposal of the technique for FCPB was prepared according to the conditions of $\#6_{up}$ coal seam and the mining conditions of the #1103 coalface. The proposal should follow these three basic principles: (1) FCPB should be carried out at the open-off cut, headgate, and tailgate of the coalface in order to enhance the effectiveness of the preconditioning; (2) at the open-off cut, the forced caving height should be two times the mining height in order to allow the caved gangues to fill in the goaf and to prevent the thick hard roof from threatening the safety of workers at the coalface; (3) FCPB of the headgate and tailgate should allow the roof to easily cave during the first weighting and prevent roof fall accidents as the coalface reached underneath the blasted roof. Practical experience suggests that the forced caving height should be larger than 2 m for the headgate and tailgate.

5.2. A Technical Proposal for Forced Caving by Presplit Blasting and Its Effectiveness

5.2.1. Forced Caving by Presplit Blasting at the Open-off Cut

(1) Layout of blastholes above the open-off cut and relevant parameters

As the mining height at #1103 coalface was 5.0 m, the height of the FCPB at the open-off cut was determined to be 10 m in accordance with the second principle described above. Parallel blastholes were drilled into the roof above the open-off cut. The blasthole mouths were arranged at 10 m intervals along a line that was parallel to, and 1 m away from, the center line of the open-off cut. The blastholes were arranged at an angle of 33° on the horizontal plane to facilitate loading them with explosives. Their length was set at 18.271 m to achieve the desired forced caving height (10 m). A total of 19 blastholes with a diameter of 90 mm were laid out in the roof along the 300 m long open-off cut for FCPB (Figure 18).

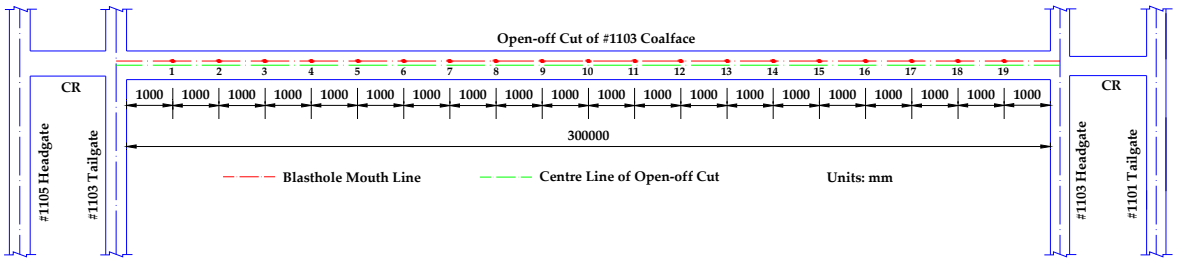

(**a**)

Figure 18. *Cont.*

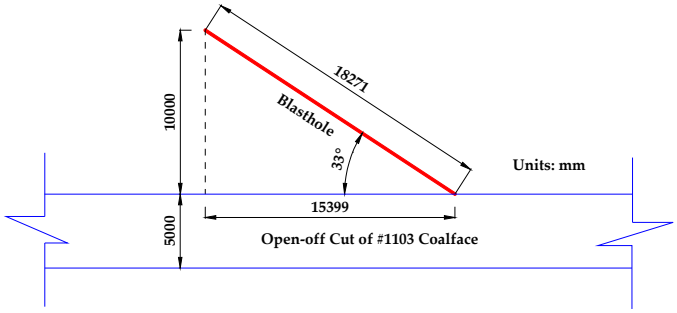

(**b**)

Figure 18. Layout of blastholes above the open-off cut and relevant parameters: (**a**) layout of blastholes; (**b**) profile of a blasthole.

(2) Loading and detonation methods

Given the great mechanical strength of the thick coarse-grained sandstone in the roof, a powerful emulsion explosive was used in this study with an attempt to achieve the expected effect. The borehole diameter was 90 mm and the decoupling coefficient (the ratio of the blasthole diameter to the charge diameter), was set at 1.2; therefore, the explosive packages were designed with a diameter of 70 mm and a length of 500 mm. Yellow mud was used as stemming for the boreholes. The ratio of charge length to stemming length was determined to be 6:4. Since the blastholes were 18.271 m long, each blasthole needed to be loaded with 10.963 m of explosives and 7.308 m of yellow mud. The explosives weighed 4 kg per meter of blasthole, which means that the explosive load carried by each blasthole was 43.848 kg. The blastholes must be cleaned before loading. During loading, a polyvinyl chloride (PVC) tube containing explosive packages, stemming, and primacord (a brand of detonating cord used in blasting) was placed into each blasthole using a tamping bar (with a diameter of 70 mm and a length of 1500 mm). Then, a wooden plug was used to block the blasthole. Figure 19 shows the schematic of a loaded blasthole. The detonators used were a type of five-stage electric delay detonator for use in coal mines. Two detonators in each blasthole were connected in parallel and the detonators in the 19 blastholes were connected in series. A high-energy exploder (MFB-1000, CBY Company, Wenzhou, China) was used to, in sequence, ignite the delay detonators and primacord in blastholes #1 through #19, with 25-millisecond delay between stages.

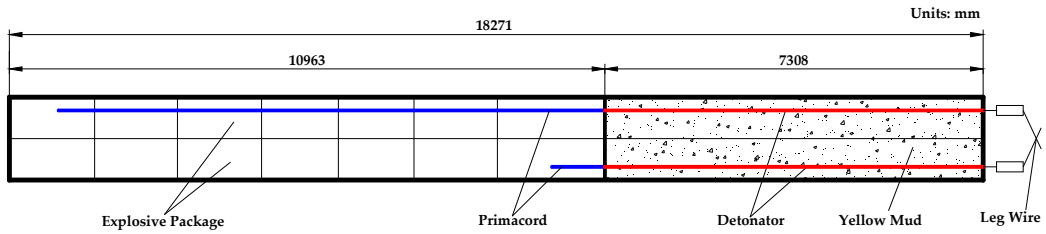

Figure 19. Schematic of a blasthole loaded with explosive.

5.2.2. Forced Caving by Presplit Blasting in the Headgate and Tailgate

(1) Layout of blastholes in the roof of the headgate and tailgate and relevant parameters

As mentioned above, the first weighting step at #1103 coalface was predicted to exceed 80 m, and the horizontal distance from the blastholes to the open-off cut was determined to be 40 m, about half the first weighting step. Two non-parallel blastholes, the top and bottom blastholes, were designed for the presplit blasting in the headgate and tailgate. To ensure the effectiveness of presplit blasting,

the vertical distance between the mouth and bottom of each top blasthole was determined to be 14 m and was set at 7 m for each bottom blasthole. The horizontal distance between the mouth and bottom of each blasthole was fixed at 50 m and all four blastholes were perpendicular to the axes of the two gates. The vertical section of each gate measured 5.0 m wide and 5.0 m high. Parameters of the blastholes were then calculated and the results were as follows: the angle between each top blasthole and the horizontal plane was 17°; the top blasthole length was 52.285 m; the height of the top blasthole mouth above the floor was 4.029 m; the angle between each bottom blasthole and the horizontal plane was 10°; the bottom blasthole length was 50.771 m; the height of bottom blasthole mouth above the floor was 3.382 m. Figure 20 shows the layout of the blastholes in the roof of the two gates and the relevant parameters.

(2) Loading method and specific parameters

Unless otherwise specified, the detonation method used to FCPB in the two gates was the same as that used at the open-off cut. Therefore, only the loading method and specific parameters are presented here. The ratio of charge length to stemming length was determined to be 6:4. For each bottom blasthole, the charge length and stemming length were 30.463 m and 20.308 m, respectively. Per meter of blasthole, the explosives weighed 4 kg. The explosive load for each bottom blasthole was calculated at 121.852 kg. Each top blasthole should be loaded with 31.371 m of explosive charge and 20.914 m of stemming. The explosive load for each top blasthole was 125.484 kg, with 4 kg per meter of blasthole.

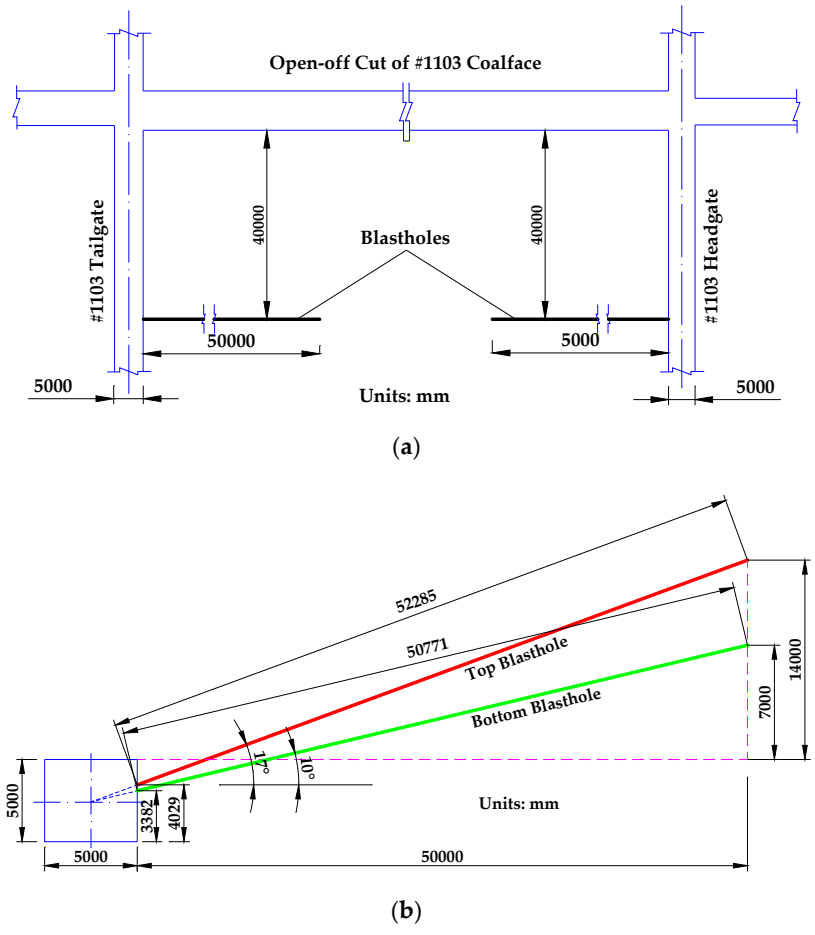

Figure 20. Layout of blastholes in the roof of the headgate and tailgate and relevant parameters: (**a**) layout of blastholes; (**b**) profile of a blasthole.

5.2.3. Implementation Results

After implementation of the technique for FCPB, the first breakage of the thick, hard main roof occurred when the coalface advanced approximately 82 m from the open-off cut. Although the safety valves of many of the HSs had already opened, the whole process of the first weighting was relatively moderate and did not produce an intense impulse load. This eliminated the possibility of worker injury and equipment damage caused by severe weighting-induced winds. Roof-associated accidents were effectively prevented and safe production was achieved. If the technique for FCPB had not been implemented, the mining height of the #1103 coalface would have been reduced. If the mining height is 3.0 m (reduced by 2.0 m), it is estimated that the use of this technique would increase coal production by about 126 kilotons. Assuming that coal is valued at 500 CNY per ton, this would bring in an additional 63 million CNY.

6. Conclusions

(1) This study proposed a new CDM for the DCCO, in order to address the deficiencies in existing detection methods. This method combines SRM, OBI and UPO into a comprehensive detection technology system, which enables spatial and temporal integration of surface, overburden, and underground detection. This method is easy to implement, highly efficient, very practical, and widely applicable, which is the novel point of the CDM.

(2) A field experiment was carried out at #1103 coalface in SCM of IMYCCL using this method. The results of the SRM suggest that the first weighting step would exceed 78 m. The results of OBI show that the first weighting step would be larger than 80 m. Through UPO, we found that the first weighting step would exceed 75 m. The results from the three approaches are generally consistent and can be used to complement each other, demonstrating the feasibility of the proposed method. It must be said, though, this new method needs to be further improved by more field experiments in similar coal mines.

(3) Based on the results of the field experiment and the mining conditions of #1103 coalface, a technique for FCPB of the roof above the open-off cut, headgate, and tailgate was developed. The technique was then applied to the coalface before the first weighting occurred. Use of this technique controlled the first weighting step to about 82 m and effectively mitigated the intensity of underground pressure behavior, thereby significantly reducing the risk of large-scale collapse of the hanging roof. The output value of the coalface was projected to increase about 63 million CNY. Therefore, this technique can offer large technical and economic benefits.

Acknowledgments: The research is financially supported by the National Natural Science Foundation of China (Nos. 51404254 and 51474206), the National Basic Research Program of China (No. 2015CB251600), the Research Fund of State and Local Joint Engineering Laboratory for Gas Drainage & Ground Control of Deep Mines (No. G201604), the Research Fund of Key Laboratory of Safety and High-efficiency Coal Mining, Ministry of Education (No. JYBSYS2015106), the Scientific Research Foundation of State Key Laboratory of Coal Mine Disaster Dynamics and Control (No. 2011DA105287-FW201602), the China Postdoctoral Science Foundation (Nos. 2014M560465 and 2015T80604), the Jiangsu Planned Projects for Postdoctoral Research Funds (No. 1302050B), the Jiangsu Qing Lan Project (No. 2016-15), the Science and Technology Foundation of Guizhou Province (No. 2015-2072) and the Natural Science Research Project of Guizhou Provincial Education Office (No. 2015-427). We wish to thank the SCM for supporting to conduct this important study, as well as Xiaofu Zhang from IMYCCL for the assistance of data collection. Special thanks are given to Mapletrans Company in Wuhan, China, for its professional English editing service. The authors are also grateful to the two anonymous reviewers for their constructive comments and helpful suggestions.

Author Contributions: All the authors contributed to publishing this paper. Wei Zhang performed the technological development and prepared the manuscript. Zhi Yang edited and revised the manuscript. Dongsheng Zhang provided theoretical guidance for the novel CDM and reviewed the manuscript. Xufeng Wang provided technical guidance for the FCPB in engineering application. Peng Li partially participated in the literatures search and data processing during the research process. Mengtang Xu performed the field experiment in SCM of IMYCCL.

Conflicts of Interest: The authors declare no conflict of interest.

References

1. Zhang, W.; Zhang, J.S.; Xu, J. Study on coal's green mining technology roadmap of Jurassic coalfield in northern Shaanxi. *Adv. Mater. Res.* **2014**, *986*, 725–729. [CrossRef]
2. Shen, L.; Gao, T.M.; Cheng, X. China's coal policy since 1979: A brief overview. *Energy Policy* **2012**, *40*, 274–281. [CrossRef]
3. Zhang, W.; Zhang, D.S.; Wu, L.X.; Wang, X.F. Numerical simulation on dynamic development features of mining-induced fractures in overlying strata during shallow coal seam mining. *Electron. J. Geotech. Eng.* **2013**, *18*, 5531–5543.
4. Jin, Z.Y.; Ma, L.Q.; Wang, F. Research progress and prospect of aquifuge in shallow coal seam: A case study in the Shendong coal field of China. *Electron. J. Geotech. Eng.* **2014**, *19*, 2809–2819.
5. Zhao, Y.S.; Du, X.L.; Yang, P.F. Discuss about the sustainable development way for China mining. *Adv. Mater. Res.* **2014**, *869*, 479–483. [CrossRef]
6. Zhang, D.S.; Fan, G.W.; Wang, X.F. Characteristics and stability of slope movement response to underground mining of shallow coal seams away from gullies. *Int. J. Min. Sci. Technol.* **2012**, *22*, 47–50. [CrossRef]
7. Karplus, V.J.; Rausch, S.; Zhang, D. Energy caps: Alternative climate policy instruments for China? *Energy Econ.* **2016**, *56*, 422–431. [CrossRef]
8. Qian, M.G. On sustainable coal mining in China. *J. China Coal Soc.* **2010**, *35*, 529–534. (In Chinese)
9. Ng, A.H.M.; Ge, L.L.; Zhang, K.; Chang, H.C.; Li, X.J.; Rizos, C.; Omura, M. Deformation mapping in three dimensions for underground mining using InSAR-southern highland coalfield in New South Wales, Australia. *Int. J. Remote Sens.* **2011**, *32*, 7227–7256. [CrossRef]
10. Chen, B.Q.; Deng, K.Z.; Fan, H.D.; Hao, M. Large-scale deformation monitoring in mining area by D-InSAR and 3D laser scanning technology integration. *Int. J. Min. Sci. Technol.* **2013**, *23*, 555–561. [CrossRef]
11. Prakash, A.; Fielding, E.J.; Gens, R.; van Genderen, J.L.; Evans, D.L. Data fusion for investigating land subsidence and coal fire hazards in a coal mining area. *Int. J. Remote Sens.* **2001**, *22*, 921–932. [CrossRef]
12. Williams, J.H.; Johnson, C.D. Acoustic and optical borehole-wall imaging for fractured-rock aquifer studies. *J. Appl. Geophys.* **2004**, *55*, 151–159. [CrossRef]
13. Meng, B.; Jing, H.W.; Chen, K.F.; Su, H.J. Failure mechanism and stability control of a large section of very soft roadway surrounding rock shear slip. *Int. J. Min. Sci. Technol.* **2013**, *23*, 127–134. [CrossRef]
14. Tan, Y.L.; Zhao, T.B.; Xiao, Y.X. In situ investigations of failure zone of floor strata in mining close distance coal seams. *Int. J. Rock Mech. Min. Sci.* **2010**, *47*, 865–870. [CrossRef]
15. Zhao, Y.X.; Jiang, Y.D. Acoustic emission and thermal infrared precursors associated with bump-prone coal failure. *Int. J. Coal Geol.* **2010**, *83*, 11–20. [CrossRef]
16. Iannacchione, A.T.; Coyle, P.R.; Prosser, L.J.; Marshall, T.E.; Litsenberger, J. Relationship of roof movement and strata-induced microseismic emissions to roof falls. *Min. Eng.* **2004**, *56*, 53–60.
17. Frid, V.; Vozoff, K. Electromagnetic radiation induced by mining rock failure. *Int. J. Coal Geol.* **2005**, *64*, 57–65. [CrossRef]
18. Kies, A.; Storoni, A.; Tosheva, Z.; Hofman, H. Radon measurements as a monitoring possibility for mining subsidence occurrence. *J. Min. Sci.* **2006**, *42*, 518–522. [CrossRef]
19. Han, D.P.; Li, D.; Shi, X.F. Effect of application of transient electromagnetic method in detection of water-inrushing structures in coal mines. *Procedia Earth Planet. Sci.* **2011**, *3*, 455–462. [CrossRef]
20. Fan, J.; Zhang, P.S.; Wu, R.X.; Guo, L.Q. Evaluating Deformation and Failure of Underground Panel's Roof Using Electric Data. Available online: http://www.mwen.info/docs/imwa_2014/IMWA2014_Fan_330.pdf (accessed on 24 September 2014).
21. Westma, E.C.; Luxbacher, K.D.; Swanson, P.L. Local earthquake tomography for imaging mining-induced changes within the overburden above a longwall mine. In Proceedings of the 42nd US Rock Mechanics Symposium (USRMS), San Francisco, CA, USA, 29 June–2 July 2008.
22. Wu, D.; Zhang, Y.L.; Liu, Y.C. Mechanical performance and ultrasonic properties of cemented gangue backfill with admixture of fly ash. *Ultrasonics* **2016**, *64*, 89–96. [CrossRef] [PubMed]
23. Lai, X.P.; Cai, M.F.; Ren, F.H.; Xie, M.W.; Esaki, T. Assessment of rock mass characteristics and the excavation disturbed zone in the Lingxin Coal Mine beneath the Xitian river, China. *Int. J. Rock Mech. Min. Sci.* **2006**, *43*, 572–581. [CrossRef]

24. Xu, Z.M.; Sun, Y.J.; Dong, Q.H.; Zhang, G.W.; Li, S. Predicting the height of water-flow fractured zone during coal mining under the Xiaolangdi Reservoir. *Min. Sci. Technol. China* **2010**, *20*, 434–438. [CrossRef]
25. Guo, H.; Yuan, L.; Shen, B.T.; Qu, Q.D.; Xue, J.H. Mining-induced strata stress changes, fractures and gas flow dynamics in multi-seam longwall mining. *Int. J. Rock Mech. Min. Sci.* **2012**, *54*, 129–139. [CrossRef]
26. Wang, J.X.; Wang, J.C.; Chen, Z.H. Movement rule of shallowly-buried thick coal seams with hard top coal and roof. *J. Min. Saf. Eng.* **2006**, *23*, 228–232. (In Chinese)
27. Ding, H.D.; Miao, X.X.; Ju, F.; Wang, X.L.; Wang, Q.C. Strata behavior investigation for high-intensity mining in the water-rich coal seam. *Int. J. Min. Sci. Technol.* **2014**, *24*, 299–304. [CrossRef]
28. Feng, G.R.; Wang, X.X.; Kang, L.X. A probe into "mining technique in the condition of floor failure" for coal seam above longwall goafs. *J. Coal Sci. Eng. China* **2008**, *14*, 19–23. [CrossRef]
29. Tian, Z.C.; Liu, Y.J.; Wang, W.C.; Ren, Y.H. Study on pressure observation of fully mechanized caving faces in coal seams with rock burst danger in Xiagou Coal Mine. *Appl. Mech. Mater.* **2014**, *580*, 1331–1334. [CrossRef]
30. Zhang, S.T.; Liu, Y. A simple and efficient way to detect the mining induced water-conducting fractured zone in overlying strata. *Energy Procedia* **2012**, *16*, 70–75. [CrossRef]
31. Antonopoulos-Domis, M.; Xanthos, S.; Clouvas, A.; Alifrangis, D. Experimental and theoretical study of radon distribution in soil. *Health Phys.* **2009**, *97*, 322–331. [CrossRef] [PubMed]
32. Zhang, D.S.; Zhang, W.; Ma, L.Q.; Wang, X.F.; Fan, G.W. Developments and prospects of detecting mining-induced fractures in overlying strata by radon. *J. Chin. Univ. Min. Technol.* **2016**, *45*, 1082–1097. (In Chinese)
33. Zhang, W.; Zhang, D.S.; Wu, L.X.; Li, J.J.; Cheng, J.X. Radon release from underground strata to the surface and uniaxial compressive test of rock samples. *Acta Geodyn. Geomater.* **2016**, *13*, 409–418. [CrossRef]
34. Zhang, W.; Zhang, D.S.; Wu, L.X.; Wang, H.Z. On-site radon detection of mining-induced fractures from overlying strata to the surface: A case study of the Baoshan Coal Mine in China. *Energies* **2014**, *7*, 8483–8507. [CrossRef]
35. Liang, S.; Li, X.H.; Mao, Y.X.; Li, C.J. Time-domain characteristics of overlying strata failure under condition of longwall ascending mining. *Int. J. Min. Sci. Technol.* **2013**, *23*, 207–211. [CrossRef]
36. Zhang, S.J.; Li, C.W.; Nie, B.S.; Zhang, H.; Sun, X.Y. Ground pressure behavior law at fully-mechanized face in Fenxi-ShuGuang coal mine. *Procedia Earth Planet. Sci.* **2009**, *1*, 275–280.
37. Winkler, R.; Ruckerbauer, F.; Bunzl, K. Radon concentration in soil gas: A comparison of the variability resulting from different methods, spatial heterogeneity and seasonal fluctuations. *Sci. Total Environ.* **2001**, *272*, 273–282. [CrossRef]
38. Banjanac, R.; Udovicic, V.; Dragic, A.; Jokovic, D.; Maletic, D.; Veselinovic, N.; Grabez, B. Daily variations of gamma-ray background and radon concentration. *Rom. J. Phys.* **2013**, *58*, 14–21.